

# Tyrosine-derived carbon dots as a highly sensitive sensor for nitroxylin in food, urine, and live cells

Hao Tang<sup>a</sup>, Jindong Dai<sup>b</sup>, Jian Shen<sup>b</sup>, Mian Zhang<sup>b</sup>, Xue Xia<sup>b</sup>, Thangamani Kanagaraj<sup>b</sup>, Dongwei Zhu<sup>b</sup>, Kanagaraj Rajalakshmi<sup>b,\*</sup>, Muthusamy Selvaraj<sup>b,\*\*</sup>, Siyi Wu<sup>c,\*\*\*</sup>, Xiaodong Zhou<sup>d,\*\*\*\*</sup>

<sup>a</sup> Department of Clinical Laboratory, Affiliated People's Hospital of Jiangsu University, 212006, Zhenjiang, Jiangsu, PR China

<sup>b</sup> Department of Immunology, Jiangsu Key Laboratory of Laboratory Medicine, School of Medicine, and School of Chemistry and Chemical Engineering, Jiangsu University, Zhenjiang, 212013, PR China

<sup>c</sup> Department of Pathology, The Affiliated Taizhou People's Hospital of Nanjing Medical University, Taizhou, 225300, Jiangsu, PR China

<sup>d</sup> Department of General Surgery, Affiliated People's Hospital of Jiangsu University, 212006, Zhenjiang, Jiangsu, PR China

## ARTICLE INFO

### Keywords:

Nitroxylin  
Tyrosine derived carbon dots  
Food samples  
Urine sample  
Cell line images

## ABSTRACT

Nitroxylin (NIT) is a commonly used veterinary medicine to treat fascioliasis in food and milk producing cattle and sheep. The residues from the edible animal food products cause severe health issues in humans. Therefore, it is of significant importance to generate an analytical approach for the detection of NIT in food products. Herein, the tyrosine derived carbon dots (T-CDs) were successfully synthesized by a simple one step hydrothermal method using tyrosine and ethylenediamine. The preparation conditions of T-CDs were optimized and analysed by UV-vis spectroscopy, fluorescence spectroscopy, PXRD, TEM, FT-IR and XPS. T-CDs shows high selectivity, good anti-interference ability (1500-fold), high sensitivity (LOD: 5.2 nM), fast response (5 min) towards the detection of NIT. T-CDs expressed contrast fluorescent confocal images depending on its concentration and NIT concentration. The detection of NIT in food samples such as cow meat, mutton, cow milk and also human urine samples was demonstrated. Good recovery results were achieved and the acquired findings were validated by HPLC detection method. All of the results prove that the present sensing strategy is simple, sensitive, selective towards NIT in food and urine samples, it provides a pathway to create an interesting new fluorescent sensor for the estimation of NIT.

## 1. Introduction

Nitroxylin (4-hydroxy-3-iodo-5-nitrobenzonitrile, NIT) is a halogenated nitrophenol, commonly used as a subcutaneous veterinary drug for the treatment of prophylaxis and control of fascioliasis in cattle and sheep [1]. Fascioliasis is a liver fluke disease (a type of parasitic worm infection) caused by *Fasciola hepatica* and *Fasciola gigantica* [2–4]. It majorly affects the fertility, milk productivity thus causing financial loss to livestock farmers [5]. Administration of NIT terminates the ATP formation via oxidative phosphorylation [6,7]. NIT exhibits higher activity than other fasciolicides in both adult and immature flukes, studies

revealed that NIT remains in animal residues even after 90 days of treatment [8]. Even though NIT has prodigious benefits to treat parasitic infections, NIT may accumulate in edible animal products such as milk and meat which leads to inauspicious effects on humans such as allergic skin, respiratory irritation, tachycardia, fever and development of bacterial resistance etc., [9]. Again, transferring even ng/L concentrations of NIT residues in water can affect the life in aquatic system [10]. NIT has been restricted in Ireland for the treatment of fluke in dairy cattle. In order to ensure the food safety, the Food and Agricultural Organization (FAO), the European Commission Regulations and the Food and Drug Administration (FDA) advised that a maximum residual limit (MRL) for

\* Corresponding authors.

\*\* Corresponding author.

\*\*\* Corresponding authors.

\*\*\*\* Corresponding author.

E-mail addresses: [rajichen89@ujs.edu.cn](mailto:rajichen89@ujs.edu.cn) (K. Rajalakshmi), [rajselva311@ujs.edu.cn](mailto:rajselva311@ujs.edu.cn) (M. Selvaraj), [2930339808@qq.com](mailto:2930339808@qq.com) (S. Wu), [zhouxdfq@hotmail.com](mailto:zhouxdfq@hotmail.com) (X. Zhou).

<https://doi.org/10.1016/j.dyepig.2025.113512>

Received 22 October 2025; Received in revised form 18 December 2025; Accepted 19 December 2025

Available online 31 December 2025

0143-7208/© 2025 Elsevier Ltd. All rights are reserved, including those for text and data mining, AI training, and similar technologies.

NIT should be lower than 400 µg per kg of animal muscle [11,12]. Therefore, it is crucial to develop an efficient sensing method for the sensitive, selective and facile detection of NIT in food samples.

Numerous sensing techniques have been established for the estimation of NIT such as liquid chromatography, mass spectrometry, gas chromatography, voltametric assay, high performance liquid chromatography, polarography and square wave voltammetry [13–19]. Unfortunately these methods have detriments in terms of need of time-consuming operation, have long response time, and need to pre-treat the sample, high-cost instrumentation, low detection limit and lack of selectivity. On the other hand, the spectrofluorimetric method overcomes the above drawbacks by providing on-site visual detection in a cost-effective manner [19–26]. Fluorescent carbon dots (CDs) are receiving huge attention for the detection of biomolecules, drugs, pesticides and food additives due to their enhanced optical properties, low cytotoxicity with high biocompatibility, prevention of reabsorption, overlap with autofluorescence and many others. A vast number of CDs have been reported for the development of electrochemical, fluorescent sensors and bioimaging applications [27–32]. CDs have been widely explored for the detection of veterinary drugs and nitroaromatic compounds due to their favourable photophysical properties and high sensitivity. CDs derived from various organic and biomass precursors have been reported for sensing antibiotics and nitro-containing drugs through fluorescence quenching mechanisms such as photoinduced electron transfer or inner filter effects. However, many of these probes show limited selectivity in complex food matrices, require longer response times, or lack validation in real biological samples. In particular, reports on CDs fluorescent sensors for nitroxylin detection remain scarce, indicating the need for alternative sensing strategies with improved selectivity and practical applicability.

Herein, we prepared tyrosine derived carbon dots (T-CDs) through a simple one step method using tyrosine, ethylene diamine and utilized for the detection of NIT. The prepared T-CDs have both positive and negative functional moieties on the surface. Considering the electron-withdrawing nitro and halogen groups present in nitroxylin, we designed a tyrosine-derived carbon dot-based fluorescent probe capable of efficient interaction with NIT. The introduction of ethylenediamine during synthesis provides surface functional groups that promote strong intermolecular interactions, leading to selective fluorescence quenching and enabling sensitive detection of NIT. The synthesis conditions were optimized as 7h reaction time with 170 °C of hydrothermal reaction temperature based on the achieving the best emission nature of the T-CDs. The formation of T-CDs was confirmed through various techniques such as UV–vis spectroscopy, emission properties, PXRD, TEM, FT-IR and XPS. The size of the T-CDs varies between 3.8 and 5.3 nm, the functional groups present on the surface were analysed through FT-IR and XPS techniques. Addition of NIT to the T-CDs causes quenching the emission behaviour of the T-CDs, from the obtained slope value of the linearity plot the lowest limit of detection (LOD) was found to be 4.9 nM. The present probe expressed high selectivity and interference ability towards NIT in the presence of 1500 fold excess of similar drugs, metal ions and anions. The bioimaging potential of the suggested probe was tested by using PC3 cell lines with three different concentrations of T-CDs and also with different concentrations of NIT. Finally, the detection of NIT was achieved in real samples such as cow meat, mutton, milk and human urine sample.

## 2. Experimental section

### 2.1. Materials

Tyrosine and 1,2-ethylenediamine were purchased from Aladdin, China. Nitroxylin, praziquantel, clenbuterol, phenothiazine, cyproheptadine, mebendazole, ractopamine, diethylcarbamazine, tensamin, anthelvet, nicarbazin, sulfamethazine, oxfendazole, fructose, glucose, galactose and sucrose were purchased from Energy Chemical Company

in China. From Hyclone (USA) the Fetal bovine serum (FBS), streptomycin, Dulbecco's phosphate buffered saline (DBS) penicillin, Roswell Park Memorial Institute (RPMI) medium 1640, Hepes buffer solution, and other cell culture materials were obtained. MTT-4,5-dimethylthiazol-2-yl)-2,5-diphenyltetrazolium bromide was obtained from Beyotime China. Benzoate, oxalate, acetate, sulfite, phosphate, fluoride, nitrate, lead ( $\text{Pb}^{2+}$ ), potassium ( $\text{K}^{+}$ ), zinc ( $\text{Zn}^{2+}$ ), mercury ( $\text{Hg}^{2+}$ ), iron ( $\text{Fe}^{3+}$ ), aluminum ( $\text{Al}^{3+}$ ), copper ( $\text{Cu}^{2+}$ ) and cadmium ( $\text{Cd}^{2+}$ ) were obtained. All other reagents were used as received as of analytical grade without additional purification. The whole experiments, the deionized water (DI) was used which was processed in our laboratory purification system.

### 2.2. Instrumentation

Cary 8454 spectrophotometer, Cary Eclipse instruments (Agilent Tech. USA) instruments were used to measure the absorption and emission spectra, respectively. Fourier transform infrared spectroscopy (FT-IR) was taken using a Thermo Nicolet 380 FT-IR spectrophotometer. A JEOL Jem advanced analytical HR-TEM was utilized for carrying out TEM images of N-CDs. Using the HI 2210 pH meter (Hanna Instruments, Woonsocket, RI, USA), the pH of the solutions was adjusted. A BioTek ELX800 microplate reader (Fisher Scientific, USA) was used to analyze the biocompatibility of T-CDs. Leica TCS SP 5 II (Leica Microsystems, USA) confocal laser scanning microscope with a 63× oil immersion objective lens with a diode laser as the light source was used to shoot live cell images.

### 2.3. Synthesis of T-CDs

The tyrosine derived carbon dots were prepared by single step *in-situ* method. In shortly, the L-tyrosine (0.05 g, 0.28 mmol; MW = 181.19 g/mol) and 1,2-ethylenediamine (0.03 g, 0.50 mmol; MW = 60.10 g/mol) were dissolved in deionized water (50 mL). Concentrated  $\text{H}_2\text{SO}_4$  (100 µL, 1.88 mmol; density = 1.84 g/mL, MW = 98.08 g/mol) was added dropwise to the mixture [29]. The forward mixture was sonicated for few minutes until to get a clear solution. The obtained transparent solution was transferred into a Teflon lined stainless steel autoclave, allowed to react for about 7h at 170 °C in the oven. The resulting yellow coloured liquid was collected, centrifuged several times at 12,000 relative centrifugal force, the supernatant liquid was collected and filtered with a pore size of 0.2 µm syringe filter. Further purification was carried out with the 3.5 KD pore size dialysis membrane for 48 h with occasional water changes. The final purified light yellow coloured T-CDs were stored at 4 °C and used for further sensing and other applications.

### 2.4. Spectroscopy measurements

The 0.4 mg/mL and 0.2 mg/mL (in DI water) T-CDs were used to measure the absorbance and emission spectra, respectively. As per the reaction conditions the amount of NIT was chosen. The probe, all the analytes were dissolved in DI water only. To verify the selectivity, each analyte was added to T-CDs separately and noted the emission response. For interference analysis, each analyte was added to the probe, NIT containing mixture and noted the emission spectra.

### 2.5. Cell culture, cytotoxicity and live cell imaging

The RPMI 1640 medium supplemented with 100 mg/mL penicillin, streptomycin and 10 % FBS was used to culture the PC3 cell lines at 37 °C with 5 %  $\text{CO}_2$  environment. In the culture dish and 96-well plates the cells were cultured for imaging and cytotoxicity analysis, respectively. Different concentrations of T-CDs (0, 0.2, 0.5, 1, 2, 5, 7, and 10 mg were dissolved in 10 mL of DI water), were added to the grown cells in 96 wells and incubated for about 24 h. The probe was then removed and the cells were gently washed with DI water then 0.5 mg/mL of MTT

was added and incubated for about 4 h. The produced formazan crystals were dissolved in 0.1 mL DMSO and observed with a BioTek ELX800 microplate reader. The cytotoxic effect of T-CDs was evaluated by using the following formula, as reported.

$$\text{Survival ratio (\%)} = (\text{Absorbance of the sample} / \text{Absorbance of the control}) \times 100$$

The 0.2 mg/mL diluted probe T-CDs were stained into the cultured cells in the 35 mm dish. The different concentration probes such as 10, 50, and 100  $\mu\text{L}$  were injected into the cultured cells for 30 min and washed with DBS. The 1 and 3  $\mu\text{M}$  of NIT solutions were injected into the probe stained cells, incubated for 10 min and carried out the fluorescence confocal studies.

## 2.6. Sample preparation for real sample analysis

The ability to detect NIT in real samples using the present probe T-CDs was tested with cow meat, lamb meat, cow milk and human urine samples. The cow meat and lamb meat samples were prepared as follows: The meat samples were purchased from the local market without any pre-treatment. The 0.5 g of meat sample was treated with known amount of NIT for 15 min. The meat sample was sonicated in DI water about 3 min and centrifuged. The supernatant liquid was collected and used for further analysis. The schematic illustration of the sample preparations is depicted in Scheme 1 [8,20,33]. The milk and urine samples were diluted into 20 times and subjected to analysis. All the experiments were done with five replicates and the mean value was taken. Using the following formula the recovery of the tests was calculated.

$$\text{Recovery (\%)} = (\text{detected amount} / \text{spiked amount}) \times 100$$

The urine samples involved in this study were checked and approved by the Ethics committee of Zhenjiang People's hospital with IRB review approval documentation number of 2025–003-02. About five volunteers we collected urine samples among them four members are in our research team. All the five members are donated their urine samples with full of their own interest without compulsion by other factors.

## 3. Results and discussions

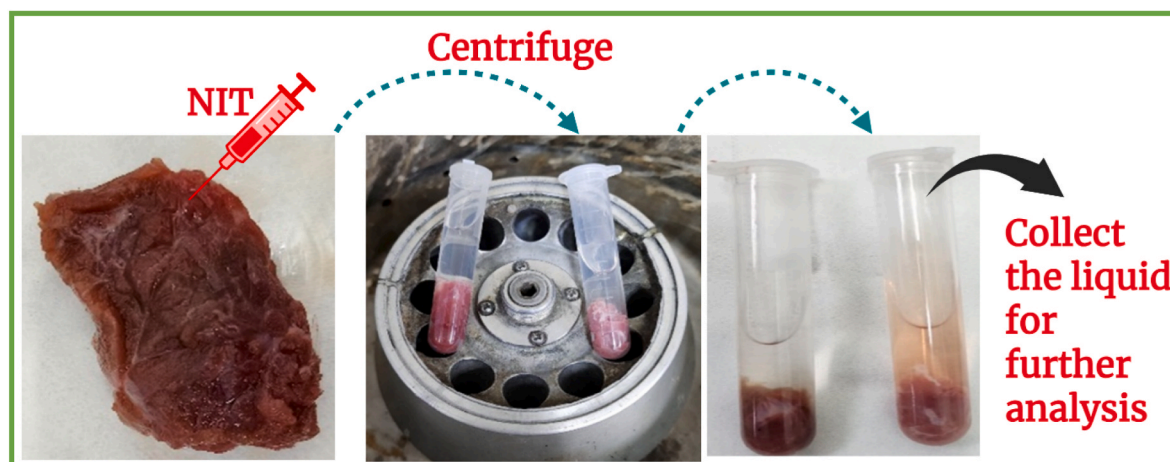
### 3.1. Preparation of T-CDs

Tyrosine and ethylene diamine were selected as precursors for the synthesis of T-CDs. Tyrosine is an amino acid, a good carbon source, is rich in heteroatoms (amine and acid functional moieties) and has both

positive and negative centres to interact with the analyte molecules strongly. Ethylene diamine is a good source of nitrogen and it is used to initiate the dots preparation through polymerization followed by carbonization process. The detailed preparation of T-CDs has been explained in Section 2.3. T-CDs was prepared through a facile single-step hydrothermal method, using the emission intensity the synthesis conditions such as reaction time and hydrothermal temperature were fixed. Initially, the excitation and emission behaviour of the prepared T-CDs was analysed (Fig. S1A), it seems the T-CDs were expressed its excitation at 352 nm, its corresponding emission profile found at 444 nm. Further, the emission performance of T-CDs at different excitation wavelengths was studied by exciting the probe from 330 to 360 nm. The 350 nm of excitation was provided the best emission profile (Fig. S1B). The best reaction time and hydrothermal reaction temperature was found by altering these phenomena and observed the emission intensity to meet a good emitting T-CDs (Fig. S1C and S1D). The rise in hydrothermal temperature from 150 °C to 170 °C, the emission peak at 444 nm was increased with slight red shift (Fig. S1C), again rising the temperature to 180 °C the emission intensity was decreased. Further, the effect of reaction time was noticed by increasing the reaction time from 5h to 8h. It seems that from 5h to 7h of reaction time, the emission intensity was increased, further increasing the reaction time there is no significant effect on the emission profile (Fig. S1D). From the above experiments, it is concluded that the hydrothermal temperature of 170 °C and 7h reaction time are the optimized reaction conditions to produce the best emitting T-CDs.

### 3.2. Characterizations of T-CDs

In order to achieve the good emitting T-CDs, the 7h reaction time with 170 °C of hydrothermal reaction temperature was kept constant for the preparation of T-CDs. The as prepared T-CDs were used for different characterizations such as XRD, TEM, XPS, sensing analysis and bio-imaging applications. As shown in Fig. 1, S1 and S2, the prepared T-CDs shows an absorbance peak at 348 nm and its corresponding emission peak appears at 444 nm with Stokes shift of 96 nm. By using rhodamine 101 as a reference molecule, the quantum yield of the T-CDs was evaluated to be 15.2 % [15,34–36]. The size and morphology of the prepared T-CDs were examined through TEM analysis. The uniformly distributed aggregation free spherical dots with size ranges of 3.8–5.3 nm were found in the TEM images (Fig. 2). The average and most populated size of T-CDs was found to be 4.4 nm. The crystalline nature of the prepared T-CDs was studied through PXRD analysis. The obtained PXRD pattern was displayed in Fig. 3A, which shows a broad band at 24.6°. It is the characteristic PXRD pattern for highly disordered carbon containing carbon dots [28]. Further, the functional groups present on the T-CDs



**Scheme 1.** Schematic illustration of NIT detection procedures in meat samples.



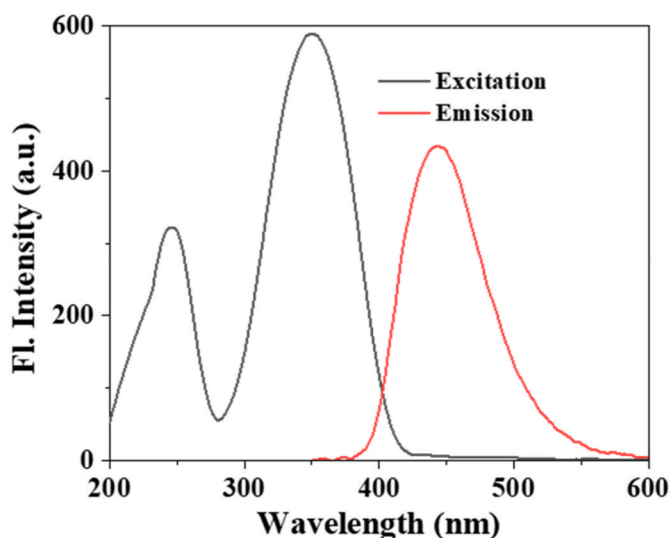


Fig. 1. Excitation and emission spectra obtained for T-CDs.

were analysed using FT-IR and XPS techniques (Fig. 3B). In the FT-IR spectrum, the strong peaks appeared at  $1280\text{ cm}^{-1}$ ,  $1475\text{ cm}^{-1}$ ,  $1685\text{ cm}^{-1}$ ,  $2880\text{ cm}^{-1}$ , and  $3330\text{ cm}^{-1}$ . The peaks appear at  $1280\text{ cm}^{-1}$ ,  $1475\text{ cm}^{-1}$  for C=O and C-N stretching vibrations, respectively. The C=C, C=O and C=N stretching vibrations were observed as joint peaks around  $1685\text{ cm}^{-1}$ . The characteristic broad and strong peak appears at  $3330\text{ cm}^{-1}$  was due to the presence of OH and  $\text{NH}_2$  functional groups [37].

Furthermore, the exact bonding nature was studied by XPS analysis, the C, N and O atoms are presented in the prepared T-CDs (Fig. 4A). In addition, the high resolution C1s spectrum consists of three peaks at 284.6 eV, 285.7 eV and 288.1 eV for C-C, C-OH and O-C=O binding modes (Fig. 4B). The N1s region was deconvoluted into three peaks at 399.2 eV, 399.9 eV and 401.1 eV for C-NH<sub>2</sub>, N-(C=O) and  $\text{NH}_4^+$  bonds, respectively (Fig. 4C). Furthermore, the O1s region shows three peaks at 530.8 eV, 531.5 eV and 535.6 eV, which are ascribed to C=O, C-O and C=O binding atmospheres (Fig. 4D), respectively [38,39]. The results are strongly suggested that, the T-CDs possess  $\text{NH}_2$ , OH and acid

functional moieties on the surface of T-CDs, which makes more convenient in the view of sensing variable targets. The chemical composition and presence of elements were analysed through CHN elemental analysis (Table S2). It is found that, the T-CDs has C = 61.7 wt%, H = 6.3 wt%, and N = 12.8 wt%. The significant nitrogen content confirms successful incorporation of nitrogen-containing functional groups from 1, 2-ethylenediamine. The high carbon content and comparatively low hydrogen reflect the formation of an aromatic/graphitic carbon core typical of carbon dots.

### 3.3. Sensing of NIT using T-CDs

Our major aim of the proposed study is to detect the NIT using T-CDs, the initial evaluation of the sensing ability of T-CDs was analysed through spectrophotometric analysis (Fig. 5A). The T-CDs shows an absorbance band at 348 nm, the absorbance peak was redshifted to 373 nm after introducing 2  $\mu\text{M}$  of NIT into the T-CDs solution. It seems that, the present probe T-CDs has good interaction with NIT and able to detect the NIT. Since the present probe T-CDs have good emission behaviour, the sensitive detection of NIT was analysed by spectrofluorometric techniques (Fig. 5B). The probe T-CDs shows an emission at 444 nm with its corresponding excitation at 350 nm. By the addition of 50 nM of NIT, the emission intensity was decreased. Further, the emission intensity was decreased linearly with a slight red shift with each addition of 50 nM of NIT (Fig. 5B). The fluorescent colour of the solution changed from bright cyan blue to less intense blue with the addition of 0.7  $\mu\text{M}$  of NIT. Under UV lamp the photographic images were taken for T-CDs and T-CDs after interacting with 0.7  $\mu\text{M}$  of NIT and the obtained images were displayed in the inset of Fig. 5B. The possible hydrogen bonding, electrostatic interactions between the  $-\text{NO}_2$ ,  $-\text{OH}$  groups present on the NIT with the functional moieties present on the T-CDs surface. Hence, the emitting nature of the T-CDs was quenched after interaction with NIT. By each addition of NIT, the emission intensity was decreased linearly and the obtained linear plot of emission intensity versus the concentration of NIT was shown in Fig. 5C. The linear regression coefficient was achieved as 0.9927 and from the slope value the LOD was found to be 5.2 nM ( $S/N = 3$ ). It is worthwhile to compare the LOD of the present method with the earlier reports as we achieved lowest LOD for NIT (Table S1).

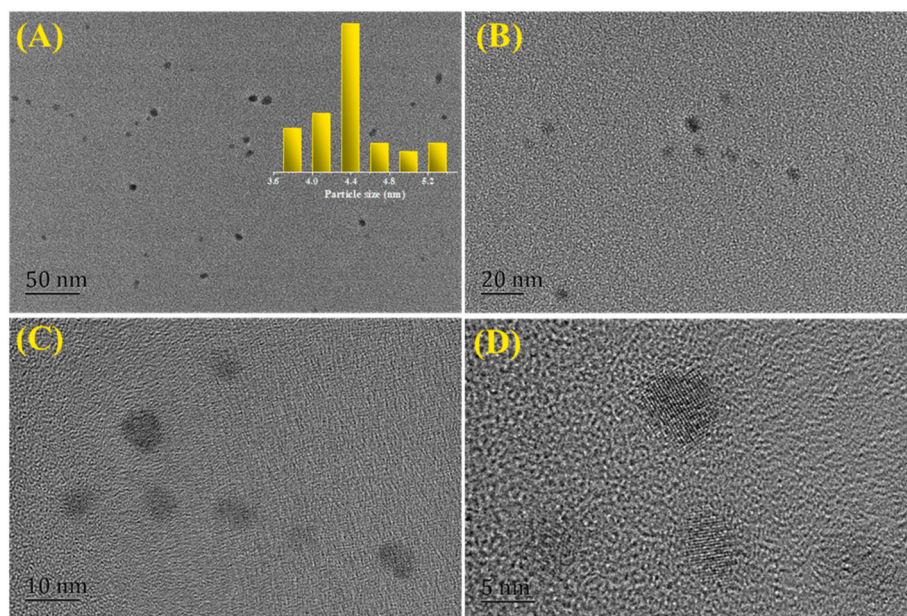


Fig. 2. (A–C) TEM images and (D) High resolution TEM image obtained for T-CDs.

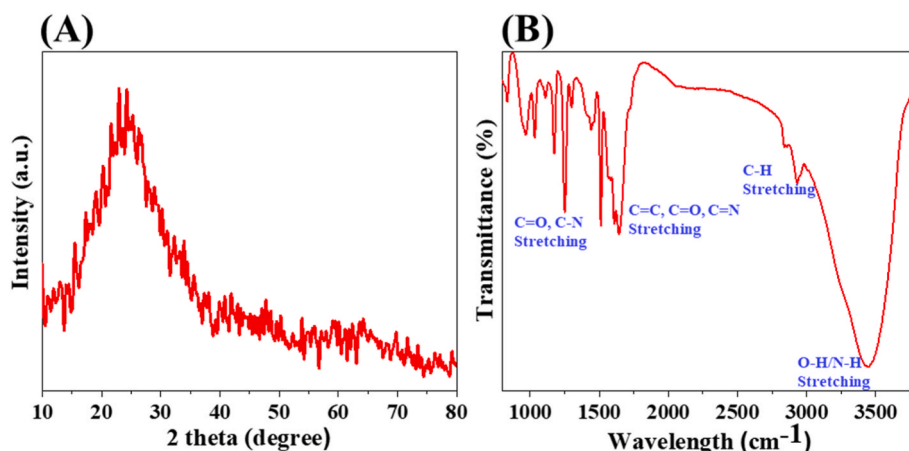


Fig. 3. Characterizations of T-CDs through (A) XRD spectrum and (B) FT-IR spectrum.

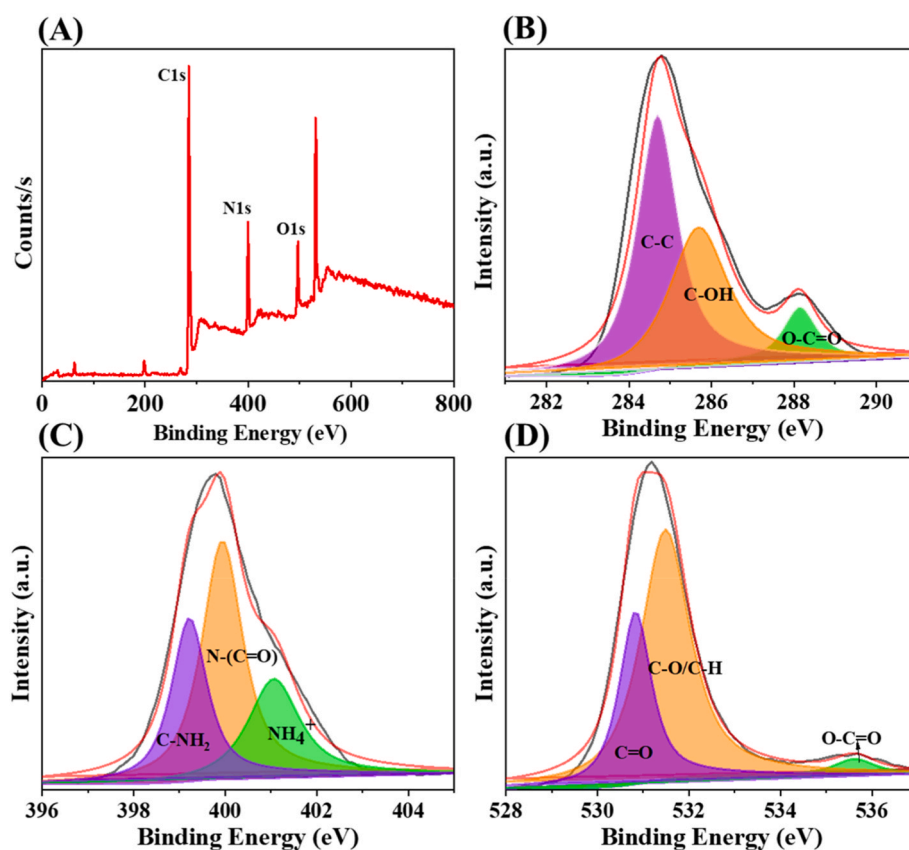
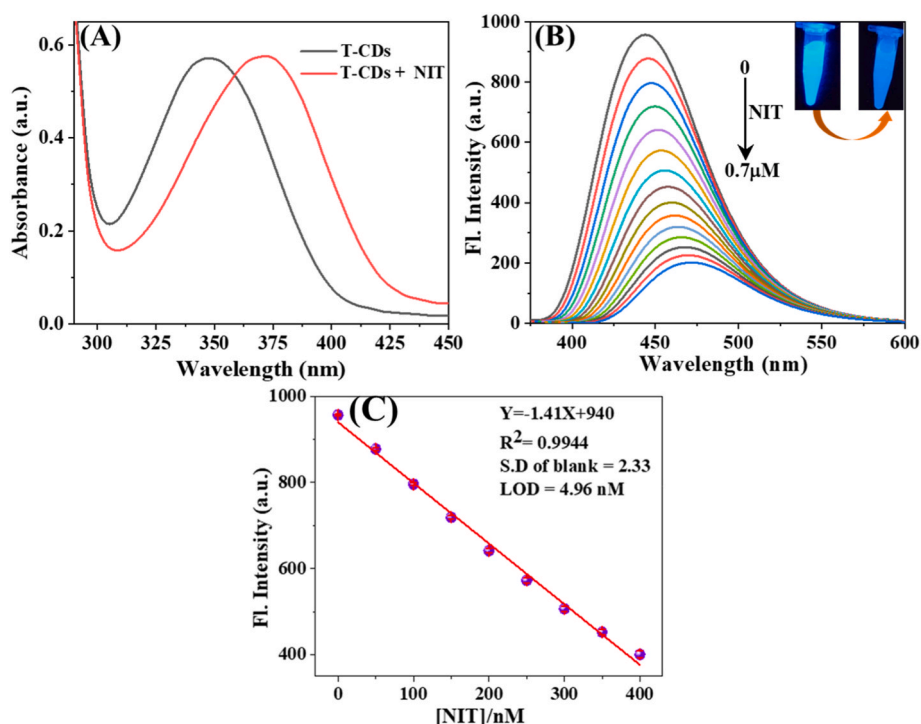


Fig. 4. XPS spectra obtained for T-CDs (A) Survey spectrum, (B–D) C1s, N1s, and O1s regions, respectively.

### 3.4. Quenching mechanism, quenching and binding constants

The quenching behaviour of T-CDs in the presence of NIT was analysed using the Stern–Volmer (SV) approach to determine the quenching and binding parameters (Fig. S3). The SV plot (Fig. S3A), constructed using the relation  $F_0/F = 1 + K_{SV}[Q]$ , exhibited a marked upward deviation from linearity at higher quencher concentrations, indicating the coexistence of both dynamic and static quenching processes. From the initial linear region, the Stern–Volmer quenching constant ( $K_{SV}$ ) was calculated as  $5.33 \times 10^6 \text{ L mol}^{-1}$ , reflecting the strong quenching capability of NIT toward T-CDs (Fig. S3B). Before examining the quenching mechanism, spectral overlap was assessed to rule out artefacts. The absorption spectrum of NIT shows minimal overlap with the

excitation and emission bands of T-CDs, indicating that inner-filter effects cannot account for the observed fluorescence suppression (Fig. 1). Furthermore, the negligible overlap between T-CDs emission and NIT absorption eliminates the possibility of Förster resonance energy transfer (FRET). A slight red-shift in the emission maximum of T-CDs was observed upon incremental addition of NIT. This bathochromic shift cannot arise from IFE or FRET; instead, it suggests subtle perturbation of the emissive surface states of T-CDs due to donor–acceptor electronic interactions. The electron-rich functional groups on T-CDs ( $-\text{OH}$ ,  $-\text{NH}_2$ ) can weakly associate with the strongly electron-deficient NIT moieties ( $-\text{NO}_2$ ,  $-\text{C} \equiv \text{N}$ , and I-substituted aromatic ring), which partially stabilises the excited state and introduces mild charge-transfer character, lowering the emission energy and producing the observed red-shift.



**Fig. 5.** (A) UV-Vis spectra obtained for T-CDs and T-CDs after interaction with 2  $\mu$ M of NIT, (B) Fluorescence emission spectra obtained for T-CDs in the presence of various concentrations of NIT (each 50 nM). Inset: Photographs obtained under UV lamp for T-CDs and its after reaction with NIT and (C) The linearity plot obtained between the fluorescence intensity against the concentration of NIT.

To clarify the quenching pathway, time-resolved fluorescence lifetime measurements were performed on T-CDs before and after NIT addition (Fig. 6). The average lifetime decreased from 6.24 ns (T-CDs) to 5.82 ns (T-CDs + NIT). As only dynamic (collisional) quenching reduces the excited-state lifetime, this measurable decrease provides direct evidence that the dominant quenching mechanism is dynamic. The donor-acceptor nature of the interacting species further supports a photoinduced charge-transfer (CT) pathway, where excited-state electrons from T-CDs transfer to the electron-deficient NIT molecules. This CT-mediated collisional process aligns with the lifetime data and explains the high quenching efficiency. The binding constant ( $K_A$ ) associated with ground-state interaction was determined using the double-

logarithmic equation  $\log[(F_0 - F)/F_0] = \log K_A + n \log [Q]$ . The corresponding linear plot (Fig. S3B) yielded a  $K_A$  value of  $5.62 \times 10^2 \text{ L mol}^{-1}$ , indicating moderate ground-state association. This agrees with the minor static component inferred from the curvature of the SV plot.

Overall, the combined steady-state, time-resolved, and electronic interaction analyses confirm that the fluorescence suppression of T-CDs by NIT occurs primarily through dynamic, photoinduced charge transfer mediated collisional quenching, with a secondary and weaker static component arising from limited ground state association. A mild excited-state stabilization responsible for the small red-shift arise from limited ground state donor acceptor interactions between T-CDs and NIT. Further, the relatively slow quenching kinetics can be attributed to a diffusion-controlled association between T-CDs and NIT. Since no chemical reaction occurs, the interaction proceeds through gradual non-covalent adsorption on the heterogeneous CD surface.

### 3.5. Optimization of detection of NIT using T-CDs

Since our aim is to selectively detect NIT among the pool of possible interferences, without being affected by its detection environment such as reaction time and pH. Generally, most sensors are affected by their detection conditions. In order to achieve an accurate, best sensing performance the detection conditions need to be studied and standardized. For this, we tested the selective detection response among the possible interferences and along with the possible interferences (Fig. S4). The N-CDs were allowed to interact with 0.5 mM of common interferences including similar drugs (Scheme S1) such as ractopamine, tensamin, tetramisole, oxfendazole, anthelvet, nicarbazin, mebendazole, phenothiazine, praziquantel, cyproheptadine, diethylcarbamazine, anions and cations which are commonly present on the environmental samples and body fluids. From Fig. S4, the results clearly indicate that the T-CDs gave a selective response towards NIT only. Again, the interference ability towards the detection of NIT using T-CDs was analysed by adding 0.7  $\mu$ M of NIT along with 10 mM of other interfering solutions. The emission intensity towards the detection of NIT was not significantly altered even

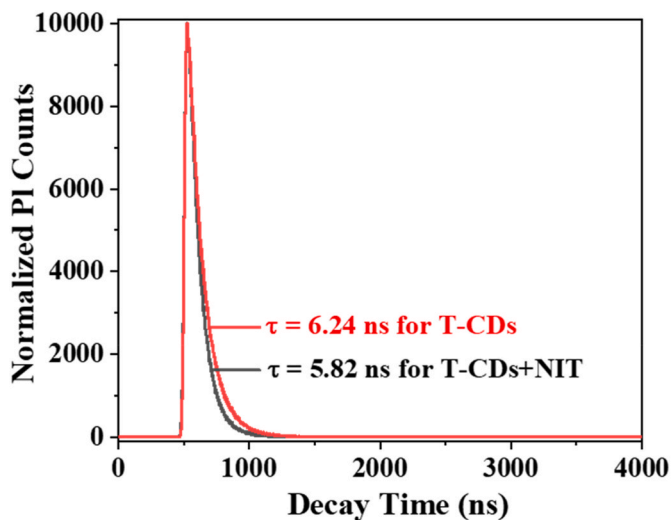


**Fig. 6.** Fluorescence life time decay curves obtained for T-CDs (red line) and T-CDs with NIT (black line). (For interpretation of the references to colour in this figure legend, the reader is referred to the Web version of this article.)



in the presence of 1500 fold excess of interferences. It indicates that the present probe T-CDs has good selectivity and good anti-interference ability towards the detection of NIT, the sensing response would not be affected by commonly presented interferences. Further stability of T-CDs and its binding with NIT at various pH was studied by measuring the emission intensity of T-CDs and T-CDs with NIT at various pH (Fig. 7A–C). The results revealed that the present probe T-CDs is highly stable in neutral pH, in both acidic and basic conditions the T-CDs is not stable (Fig. 7A–C). This might be the functional groups present on the surface of the T-CDs were hydrogenated or dehydrogenated in acidic and basic environments and also the highest sensing ability was also achieved at neutral pH. This will be benefitted during the detection of NIT in biological samples. The detection time of NIT using T-CDs was analysed by introducing various concentrations of NIT in T-CDs. The emission response was observed, the plot of emission intensity versus the response time was drawn (Fig. 7D). It seems that, the emission intensity dropped immediately by introducing each concentration of NIT and attained plateau about 5 min for all the concentrations of NIT. Hence, the reaction time of 5 min is acceptable for the detection of NIT using the present probe T-CDs.

### 3.6. Fluorescence bioimaging using T-CDs

All the above outcome results led us to extend the application of T-CDs towards NIT detection in cell lines via fluorescent bioimaging. Before introducing the probe solution to the living cells, the survival ratio of the living cells against the probe solution was tested using the regular MTT assay method. The PC3 cell lines were cultured in a 96-well plate and the different concentrations of the present probe T-CDs were introduced into the grown cell wells. The obtained cell survival ratio was plotted against the concentration of the probe solution and displayed in Fig. S5. About 90 % of the cells were live even when treated with 10 mg T-CDs, the high survival ratio of the cells indicates that the present probe T-CDs has good biocompatibility and will be benefit as a good bioimaging reagent. Fig. 8 shows the fluorescence confocal bioimages

obtained for PC3 cells stained with different concentrations of probe T-CDs and then treated with NIT. Initially, the well grown PC3 cells were treated with 10, 50, and 100  $\mu\text{L}$  of probe solutions (0.2 mg/mL) (I, II and III, respectively). The bright blue fluorescent images were obtained as shown in Fig. 8A–D, and G. The different concentrations treated three types of probe-stained cells were further exposed with 1  $\mu\text{M}$  (Fig. 8B–E, and H) and 3  $\mu\text{M}$  of NIT (Fig. 8C–F, and I). After treatment with NIT, the fluorescence intensity of the cells was decreased, the intensity varies with the concentrations of the NIT. It is noted that, the concentrations of the probe solution do not provide significant impact towards the detection of NIT in live cells, i.e. even at low concentration probe can provide contrast images and there are no significant differences observed in Fig. 8C–F and I. These findings suggest that T-CDs can be a good bioimaging reagent and can produce contrast images with different NIT concentrations.

### 3.7. Determination of NIT in injection, meat, milk and urine samples

Based on the obtained interesting results, the developed probe for the detection of NIT was applied to the estimation of NIT in various real samples such as commercial injection, lamb meat, cow meat, and cow milk and also in human urine samples. The injection “Dovix” was subjected to the analysis, the known amount of 20, 50 and 100 nM of NIT was added to the probe solution. Based on the obtained calibration curve, the amount of NIT present in the sample was determined. It seems that the present method of detection shows high recovery results based on the added amount of commercial drug Dovix (Table 1). The cow meat, lamb meat, cow milk and human urine samples were collected as explained in Section 2.7, Scheme 1. As NIT is used as a veterinary medicine the detection of NIT in human edible meat samples, milk samples and human urine samples is of concern. It is mentioned that the regulatory limits of NIT on the type of meat and milk samples are 20 and 20–400  $\mu\text{g kg}^{-1}$  (depending on the meat such as kidney, liver, muscle and fat) as per the European Commission Regulation number 997/1999 [33,40]. The real sample analysis results indicated that the proposed

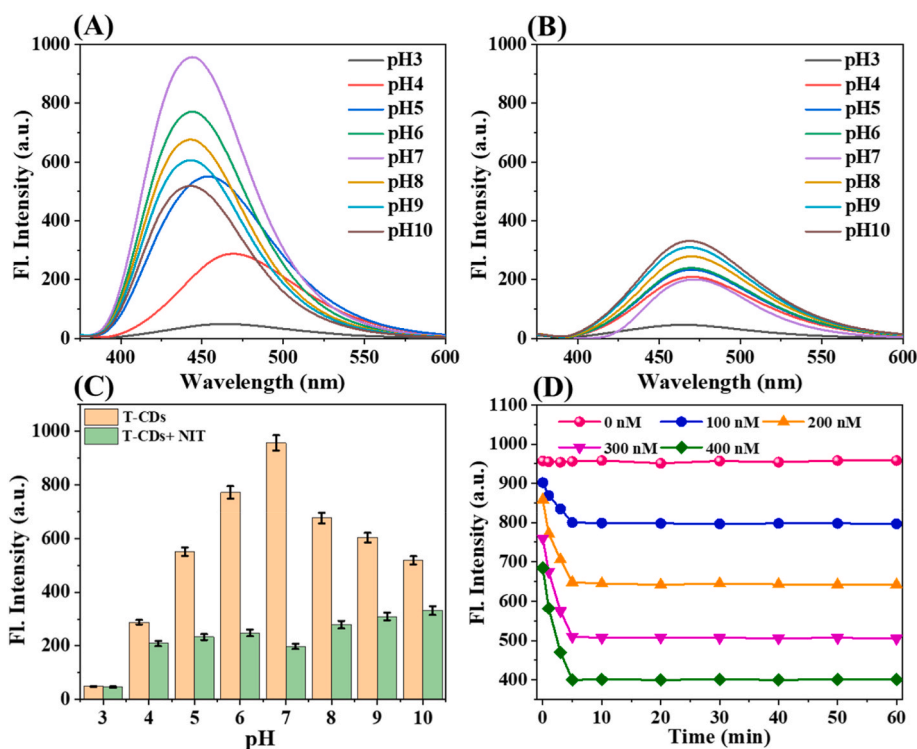


**Fig. 7.** Effect of pH on T-CDs (A) in the absence (B) in presence of 0.7  $\mu\text{M}$  of NIT, (C) its bar chart representation and (D) Plot of fluorescence emission intensity versus reaction time obtained for T-CDs in the presence of different concentrations of NIT.

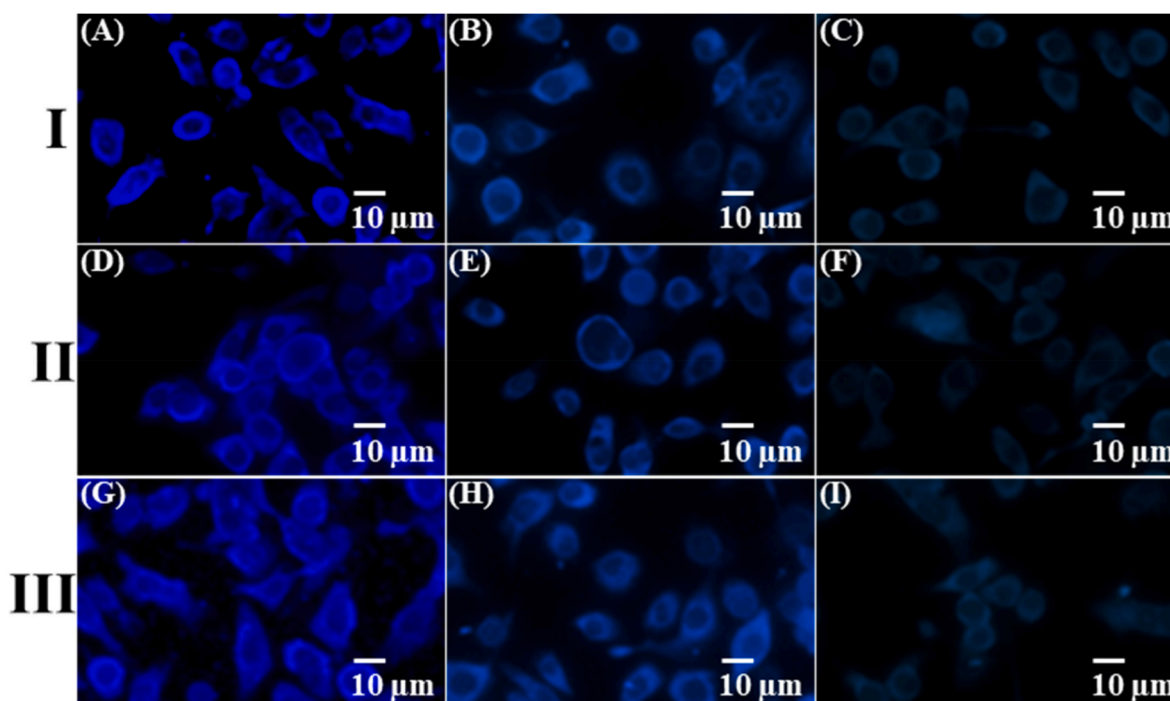


**Fig. 8.** Fluorescent confocal microscopic images of PC3 cell lines: (A,D,G) PC3 cells treated with 10, 50 and 100  $\mu$ L of T-CDs (0.2 mg/mL) only. (B,E,H) T-CDs stained cells treated with 1  $\mu$ M of NIT. (C,F,I) T-CDs stained cells treated with 3  $\mu$ M of NIT.

**Table 1**

Detection of NIT in food and urine samples using T-CDs (n = 5).

Samples	NIT spiked (nM)	NIT measured (nM)		Recovery (%)
		Fluorimetry method	HPLC method	
Dovix injection	20	19.8	19.2	99.0
	50	49.7	49.2	99.4
	100	99.98	99.90	99.98
Lamb meat	20	19.9	19.0	99.5
	50	49.8	49.2	99.6
	100	99.9	99.7	99.9
Cow meat	20	20.05	19.5	100.25
	50	50.01	49.4	100.02
	100	100.02	99.97	100.02
Cow milk	20	19.7	19.1	98.5
	50	49.6	49.5	99.2
	100	99.7	99.5	99.7
Human urine	20	19.7	19.5	98.5
	50	49.7	49.8	99.4
	100	99.6	99.5	99.6

present sensor is suitable for the detection of NIT in food and urine samples. The recovery results obtained for spiked NIT in lamb meat was from 99.5 % to 99.9 %, in cow meat was from 100.02 % to 100.25 %, in cow milk was from 98.5 % to 99.7 % and in human urine samples was from 98.5 % to 99.6 %. The present probe has good recovery with the spiked amount of NIT, which revealed that the present probe T-CDs could be used for the estimation of NIT in food samples and urine samples. Further, the obtained results were validated with HPLC method.

#### 4. Conclusions

The proposed probe T-CDs was successfully synthesized by using tyrosine and ethylenediamine as precursors. The emission peak was observed at 444 nm with corresponding excitation at 352 nm. Based on

its emission peak, the reaction conditions were optimized to achieve good emitting T-CDs as 7h reaction time with 170 °C of hydrothermal reaction temperature. The successful formation of T-CDs, their size, shape, surface functional groups and bonding nature were analysed through UV-vis spectroscopy, emission properties, PXRD, TEM, FT-IR, and XPS. The sizes of the T-CDs varied from 3.8 to 5.3 nm, and the average size of the T-CDs was found to be 4.4 nm. By introducing each concentration of NIT into the T-CDs the emission nature was quenched linearly, based on the slope value obtained from the linearity curve, the LOD was found to be 5.2 nM. T-CDs shows high selectivity among the pool of similar drugs, common interfering ions and high interference tolerance ability. Even in the presence of 1500 fold excess of interfering compounds, T-CDs selectively detects NIT. T-CDs displayed contrast bioimages depends on both concentration of probe solution as well as presence of different concentration of NIT. Since, NIT is present on the food residues of anthelmintics the cow meat, mutton meat, milk samples were tested for the ability to detect the NIT. Moreover, the NIT detection was also tested in human urine samples and achieved good recovery results. The present method of detection was validated by HPLC method. Finally, through a simple preparation method a highly biocompatible probe T-CDs were prepared and delivered a highly sensitive, selective detection of NIT. The detection in meat sample, milk and urine samples was demonstrated. The present work encourages the researchers to find the simplest way to sensitively detect the harmful drugs in food samples.

#### CRediT authorship contribution statement

**Hao Tang:** Writing – review & editing, Writing – original draft, Visualization, Validation, Funding acquisition. **Jindong Dai:** Writing – review & editing, Writing – original draft, Visualization, Validation. **Jian Shen:** Writing – review & editing, Writing – original draft, Resources, Project administration, Methodology. **Mian Zhang:** Writing – review & editing, Writing – original draft, Visualization, Validation. **Xue Xia:** Writing – review & editing, Writing – original draft, Visualization, Validation. **Thangamani Kanagaraj:** Writing – review & editing, Writing – original draft, Visualization, Validation, Supervision. **Dongwei Zhu:** Writing – review & editing, Writing – original draft, Resources,



Project administration, Methodology. **Kanagaraj Rajalakshmi**: Methodology, Investigation, Formal analysis, Data curation, Conceptualization. **Muthusamy Selvaraj**: Writing – review & editing, Writing – original draft, Formal analysis, Data curation, Conceptualization. **Siyi Wu**: Writing – review & editing, Writing – original draft, Visualization, Validation. **Xiaodong Zhou**: Writing – review & editing, Writing – original draft, Methodology, Investigation, Funding acquisition.

## Ethical statement

The urine samples involved in this study were checked and approved by the Ethics committee of Zhenjiang People's hospital with IRB review approval documentation number of 2025–003-02. About five volunteers we collected urine samples among them four members are in our research team. All the five members are donated their urine samples with full of their own interest without compulsion by other factors.

## Disclosure statement

No potential conflict of interest was reported by the author(s).

## Declaration of competing interest

The authors declare that they have no known competing financial interests or personal relationships that could have appeared to influence the work reported in this paper.

## Acknowledgements

The authors thanks to the financial supports from Jinshan Elite Talents in the Medical Field (JSYC2023-008), Beijing Bethune Medical Science Research Fund (2023-YJ-119-J-033), Zhenjiang Science and Technology Plan - Social Development (SH2024047) and Zhenjiang City Science and Technology Plan - Basic Research Project (JC2025044).

## Appendix A. Supplementary data

Supplementary data to this article can be found online at <https://doi.org/10.1016/j.dyepig.2025.113512>.

## Data availability

No data was used for the research described in the article.

## References

- [1] Zhou J-W, Zou X-M, Song S-H, Chen G-H. Quantum dots applied to methodology on detection of pesticide and veterinary drug residues. *J Agric Food Chem* 2018;66:1307–19. <https://doi.org/10.1021/acs.jafc.7b05119>.
- [2] Baiak BHB, Lehnen CR, da Rocha RA. Anthelmintic resistance in cattle: a systematic review and meta-analysis. *Livest Sci* 2018;217:127–35. <https://doi.org/10.1016/j.livsci.2018.09.022>.
- [3] Kaminsky R, Ducray P, Jung M, Clover R, Rufener L, Bouvier J, Weber SS, Wenger A, Wieland-Berghausen S, Goebel T, Gauvry N, Pautrat F, Skripsky T, Froelich O, Komoin-Oka C, Westlund B, Sluder A, Mäser P. A new class of anthelmintics effective against drug-resistant nematodes. *Nature* 2008;452:176–80. <https://doi.org/10.1038/nature06722>.
- [4] Ghoneim MM, El-Ries M, Hassanein AM, Abd-Elaziz AM. Voltammetric assay of the anthelmintic veterinary drug nitroxylin in bulk form and formulation at a mercury electrode. *J Pharm Biomed Anal* 2006;41:1268–73. <https://doi.org/10.1016/j.jpba.2006.03.022>.
- [5] Wang W, Fan B, Zhang X, Guo R, Zhao Y, Zhou J, Zhou J, Peng Q, Zhu M, Li J. Development of a colloidal gold immunochromatographic assay strip using monoclonal antibody for rapid detection of porcine deltacoronavirus. *Front Microbiol* 2023;13:1074513. <https://www.frontiersin.org/journals/microbiology/articles/10.3389/fmicb.2022.1074513/full>.
- [6] Liang Q, Chalamaiiah M, Liao W, Ren X, Ma H, Wu J. Zein hydrolysate and its peptides exert anti-inflammatory activity on endothelial cells by preventing TNF- $\alpha$ -induced NF- $\kappa$ B activation. *J Funct Foods* 2020;64:103598. <https://doi.org/10.1016/j.jff.2019.103598>.
- [7] Yuan L, Lin J, Peng Y, Gao R, Sun Q. Chlorantraniliprole induces adipogenesis in 3T3-L1 adipocytes via the AMPK $\alpha$  pathway but not the ER stress pathway. *Food Chem* 2020;311:125953. <https://doi.org/10.1016/j.foodchem.2019.125953>.
- [8] Ekström L-G, Slanina P. Determination and health-risk evaluation of nitroxylin residues in the edible tissue of cattle. *Acta Vet Scand* 1982;23:313–24. <https://doi.org/10.1186/BF03546783>.
- [9] Mesfin YM, Mitiku BA, Tamrat Admasu H. Veterinary drug residues in food products of animal origin and their public health consequences: a review. *Vet Med* 2024;10:e70049. <https://doi.org/10.1002/vms3.70049>.
- [10] Na G, Hu X, Yang J, Sun Y, Kwee S, Tang L, Xing G, Xing Y, Zhang G. A rapid colloidal gold-based immunochromatographic strip assay for monitoring nitroxylin in milk. *J Sci Food Agric* 2020;100:1860–6. <https://doi.org/10.1002/jsfa.10074>.
- [11] Okocha RC, Olatoye IO, Adedeji OB. Food safety impacts of antimicrobial use and their residues in aquaculture. *Public Health Rev* 2018;39:21. <https://doi.org/10.1186/s40985-018-0099-2>.
- [12] Salim MM, Ashraf S, Hashem HM, Belal F. Voltammetric estimation of residual nitroxylin in food products using carbon paste electrode. *Sci Rep* 2022;12:14289. <https://doi.org/10.1038/s41598-022-18305-6>.
- [13] Whelan M, Bloemhoff Y, Furey A, Sayers R, Danaher M. Investigation of the persistence of nitroxylin residues in milk from lactating dairy cows by ultra performance liquid chromatography Tandem Mass spectrometry. *J Agric Food Chem* 2011;59:7793–7. <https://doi.org/10.1021/jf202050r>.
- [14] Jung H-N, Park D-H, Yoo K-H, Cho H-J, Shim J-H, Shin H-C, Abd El-Aty AM. Simultaneous quantification of 12 veterinary drug residues in fishery products using liquid chromatography-tandem mass spectrometry. *Food Chem* 2021;348:129105. <https://doi.org/10.1016/j.foodchem.2021.129105>.
- [15] Muthusamy S, Yin S, Rajalakshmi K, Meng S, Zhu D, Xie M, Xie J, Lodi RS, Xu Y. Development of a quinoline-derived turn-on fluorescent probe for real time detection of hydrazine and its applications in environment and bioimaging. *Dyes Pigments* 2022;206:110618. <https://doi.org/10.1016/j.dyepig.2022.110618>.
- [16] Wu Y, Li Z, Zhu H, Zi R, Xue F, Yu Y. Identification of Tartary buckwheat (*Fagopyrum tataricum* (L.) Gaertn) and common buckwheat (*Fagopyrum esculentum* Moench) using gas chromatography–mass spectroscopy-based untargeted metabolomics. *Foods* 2023;12:2578. <https://doi.org/10.3390/foods12132578>.
- [17] Yao L, Xu J, Zhang L, Liu L, Zhang L. Nanoencapsulation of anthocyanin by an amphiphilic peptide for stability enhancement. *Food Hydrocoll* 2021;118:106741. <https://doi.org/10.1016/j.foodhyd.2021.106741>.
- [18] Tang S, Dong S, Chen M, Gao R, Chen S, Zhao Y, Liu Z, Sun B. Preparation of a fermentation solution of grass fish bones and its calcium bioavailability in rats. *Food Funct* 2018;9:4135–42. <https://doi.org/10.1039/C8FO00674A>.
- [19] Li Y, Sun J, Wu X, Chen Q, Lu B, Dai C. Detection of viability of soybean seed based on fluorescence hyperspectra and CARS-SVM-AdaBoost model. *J Food Process Preserv* 2019;43:e14238. <https://onlinelibrary.wiley.com/doi/abs/10.1111/jfpp.14238>.
- [20] Lu C-Z, Wang C-Y, Song C, Qin T, Lv T, Zeng C, Chen S, Xu Z, Xun Z, Liu B, Wang Y-L, Zhu M-Q. A ratiometric fluorescent indicator-displacement assay for on-site determination and intracellular imaging of nitroxylin. *Food Chem* 2024;435:137617. <https://doi.org/10.1016/j.foodchem.2023.137617>.
- [21] Xu Z, Song C, Chen Z, Zeng C, Lv T, Wang L, Liu B. A portable paper-based testing device for fast and on-site determination of nitroxylin in food. *Anal Chim Acta* 2023;1260:341201. <https://doi.org/10.1016/j.aca.2023.341201>.
- [22] Zhou M, Song C, Qin T, Xun Z, Liu B. Fast and sensitive detection of nitroxylin using a chalcone-based supramolecular fluorescent sensor. *Spectrochim Acta Mol Biomol Spectrosc* 2023;302:122974. <https://doi.org/10.1016/j.saa.2023.122974>.
- [23] Gan Z, Hu X, Xu X, Zhang W, Zou X, Shi J, Zheng K, Arslan M. A portable test strip based on fluorescent europium-based metal–organic framework for rapid and visual detection of tetracycline in food samples. *Food Chem* 2021;354:129501. <https://doi.org/10.1016/j.foodchem.2021.129501>.
- [24] Wang Y, Xu J, Qiu Y, Li P, Liu B, Yang L, Barnych B, Hammock BD, Zhang C. Highly specific monoclonal antibody and sensitive quantum dot beads-based fluorescence immunochromatographic test strip for tebuconazole assay in agricultural products. *J Agric Food Chem* 2019;67:9096–103. <https://pubs.acs.org/doi/abs/10.1021/acs.jafc.9b02832>.
- [25] Liang N, Hu X, Li W, Mwakosya AW, Guo Z, Xu Y, Huang X, Li Z, Zhang X, Zou X. Fluorescence and colorimetric dual-mode sensor for visual detection of malathion in cabbage based on carbon quantum dots and gold nanoparticles. *Food Chem* 2021;343:128494. <https://doi.org/10.1016/j.foodchem.2020.128494>.
- [26] Jun S, Xin Z, Hanping M, Xiaohong W, Xiaodong Z, Hongyan G. Identification of pesticide residue level in lettuce based on hyperspectra and chlorophyll fluorescence spectra. *Int J Agric Biol Eng* 2016;9:231–9. <https://ijabe.org/index.php/ijabe/article/view/2519>.
- [27] Huang X, Liu Z, Huang Y, Zong Y, Yang X, Hu Z, Zeng C. One-pot room temperature synthesis of orange-emitting carbon dots for highly-sensitive vitamin B12 sensing. *Spectrochim Acta Mol Biomol Spectrosc* 2022;276:121239. <https://doi.org/10.1016/j.saa.2022.121239>.
- [28] Zhu D, Dai J, Jia J, Kanagaraj T, Rajalakshmi K, Muthusamy S, Geng L, Yuan G. Biogenic synthesis of N-doped carbon dots from S. cumini seeds for prostate cancer biomarker citrate detection, its live cancer cell imaging. *Spectrochim Acta Mol Biomol Spectrosc* 2025;329:125568. <https://doi.org/10.1016/j.saa.2024.125568>.
- [29] Rajalakshmi K, Deng T, Muthusamy S, Xie M, Xie J, Lee K-B, Xu Y. Prostate cancer biomarker citrate detection using triaminoguanidinium carbon dots, its applications in live cells and human urine samples. *Spectrochim Acta Mol Biomol Spectrosc* 2022;268:120622. <https://doi.org/10.1016/j.saa.2021.120622>.
- [30] Zhang C, Yu X, Shi X, Han Y, Guo Z, Liu Y. Development of carbon quantum dot-labeled antibody fluorescence immunoassays for the detection of morphine in

- hot pot soup base. *Food Anal Methods* 2020;13:1042–9. <https://link.springer.com/article/10.1007/s12161-020-01700-y>.
- [31] Hu X, Shi J, Shi Y, Zou X, Arslan M, Zhang W, Huang X, Li Z, Xu Y. Use of a smartphone for visual detection of melamine in milk based on Au@ Carbon quantum dots nanocomposites. *Food Chem* 2019;272:58–65. <https://doi.org/10.1016/j.foodchem.2018.08.021>.
- [32] Hu X, Shi J, Shi Y, Zou X, Tahir HE, Holmes M, Zhang W, Huang X, Li Z, Xu Y. A dual-mode sensor for colorimetric and fluorescent detection of nitrite in hams based on carbon dots-neutral red system. *Meat Sci* 2019;147:127–34. <https://doi.org/10.1016/j.meatsci.2018.09.006>.
- [33] Abd Elhaleem SM, Belal F, El-Shabrawy Y, El-Maghrabey M. Self-ratiometric fluorescence approach based on room-temperature instantaneously synthesized carbon dots from Folin's reagent and ethanolamine for determination of nitroxinil in water, milk, and food samples. *Anal Chim Acta* 2024;1323:343061. <https://doi.org/10.1016/j.aca.2024.343061>.
- [34] Muthusamy S, Rajalakshmi K, Kannan P, Zhu D, Seo Y, Zhu W, Song J-W, Lee K-B, Nam Y-S. Targeting citrate as novel strategy in diagnosing prostate cancer using Rhodamine extended red emissive fluorophore: sensing mechanism and prostate tumor diagnosis applications. *Sensor Actuator B Chem* 2022;369:132299. <https://doi.org/10.1016/j.snb.2022.132299>.
- [35] Muthusamy S, Rajalakshmi K, Zhu D, Zhao L, Wang S, Zhu W. A novel lysosome targeted fluorophore for H2S sensing: enhancing the quantitative detection with successive reaction sites. *Sensor Actuator B Chem* 2020;320:128433. <https://doi.org/10.1016/j.snb.2020.128433>.
- [36] Muthusamy S, Rajalakshmi K, Zhu D, Zhu W, Wang S, Lee K-B, Xu H, Zhao L. Dual detection of mercury (II) and lead (II) ions using a facile coumarin-based fluorescent probe via excited state intramolecular proton transfer and photo-induced electron transfer processes. *Sensor Actuator B Chem* 2021;346:130534. <https://doi.org/10.1016/j.snb.2021.130534>.
- [37] Rajalakshmi K, Abraham John S. Chemical attachment of functionalized multiwalled carbon nanotubes on glassy carbon electrode for electrocatalytic application. *Electrochim Acta* 2015;165:268–76. <https://doi.org/10.1016/j.electacta.2015.01.108>.
- [38] Guo X, Zhang X, Wang Y, Tian X, Qiao Y. Converting furfural residue wastes to carbon materials for high performance supercapacitor. *Green Energy Environ* 2022;7:1270–80. <https://doi.org/10.1016/j.gee.2021.01.021>.
- [39] Rajalakshmi K, John SA. Functionalized multiwalled carbon nanotubes-nanostructured conducting polymer composite modified electrode for the sensitive determination of uricase inhibitor. *Electrochim Acta* 2015;173:506–14. <https://doi.org/10.1016/j.electacta.2015.05.101>.
- [40] Takeba K, Matsumoto M, Nakazawa H. Determination of nitroxynil in cow milk by reversed-phase high-performance liquid chromatography with dual-electrode coulometric detection. *J Chromatogr A* 1992;596:67–71. [https://doi.org/10.1016/0021-9673\(92\)80203-7](https://doi.org/10.1016/0021-9673(92)80203-7).